Synthesis, optical and AC electrical characteristics of nanocomposites (Bi$_2$O$_3$/ZnO) films prepared by thermal evaporation technique

H. S. Suhail, A. R. Abdulridha
University of Babylon, College of Education for Pure Sciences, Department of Physics , Iraq

In this paper, pure bismuth oxide (Bi$_2$O$_3$) and ZnO-doped with a ratio of (0, 0.12, 0.24, 0.36 and 0.48 wt.%) thin films are prepared by thermal evaporation methods under pressure 1×10^{-7} bar with a rate of deposition 0.5 nm.s^{-1}, at ambient temperature on glass substrates (RT) with thickness 50 nm and annealed at temperature 573 K for 2 hours. The phase structures of Bi$_2$O$_3$ (monoclinic) and Bi$_2$O$_3$/ZnO NCPs are confirmed by X-ray diffraction (XRD) investigation. The concentration of ZnO-doping reduces the average crystallite size from 17,35 nm to 8.67 nm. Moreover, using XRD data, the average strain, stress, and dislocation density values are computed. The spectroscopy techniques such as Fourier transform infrared (FT-IR) and scanning electron microscopy with field emission probes were used to examine the structures. The FT-IR results showed no chemical interactions between the (Bi$_2$O$_3$/ZnO) NPs. The results of the field emission-scanning electron microscope (FE-SEM) analysis the (Bi$_2$O$_3$/ZnO) NPs were distributed uniformly throughout. The actually result of optical characteristics for (Bi$_2$O$_3$/ZnO) showed that the absorbance, and absorption coefficient, increase with the increased concentrations of (ZnO). At the same time, the transmittance and energy band gaps were decreased with a rise in concentrations (ZnO) that have a high ability to absorb UV-light. The dielectric characteristics were checked in the frequency range from 100 Hz to 5 MHz. The results of the insulating characteristics showed that the dielectric constant and the dielectric loss of thin films (Bi$_2$O$_3$/ZnO) decreased with increasing frequency. In contrast, they increase when the concentration of (ZnO NPs) increases. The A.C conductivity of the thin films (Bi$_2$O$_3$/ZnO) increases with the frequency and concentration of (ZnO) NPs. Finally, the structural and insulating results the indicated characteristics of the (Bi$_2$O$_3$/ZnO) thin films may be helpful in various nano-electronic devices and sensors.

1. Introduction

Over the past hundred years, the field of nanotechnology has grown a lot. And now, many different kinds of research are linked to nanotechnology in some way. Nanotechnology is a developing, synthesizing, characterizing and putting materials to use and gadgets through a change in dimensions and the form of the nanoscale "nano" prefix is used at the beginning of each stream used even in product advertisements, as a keyword [1]. Nanotechnology's applications Nanotechnology is being used in nearly every field of science and technology [2]. Nanoscience, as opposed to nanotechnology, focuses on the arrangement and fundamental characteristics of atoms at the nanoscale. Nanotechnology, on the other hand, is a technique for controlling matter at the atomic level to synthesize novel nanomaterials with different characteristics [3]. In at least one of these dimensions, nanomaterials are substances less than 100 nm in size. To put it another way, this suggests that they have a lot of a significantly Microscale is smaller. Nanomaterials are one billionth of a meter in size, with an average size of 10^{-9} m. The physicochemical characteristics of the nanoparticles differ from those of the bulk material's size and shape are intrinsically linked.

At the nanoscale level the shape and size of the nanomaterials creates a distinct character that has new traits as well as new capabilities [4]. In the last few decades, the human population has grown rapidly, which has led to a rapid expansion of industry and the use of automobiles. The outcome is a proliferation of harmful and hazardous chemical species that pose a serious threat to human health and the environment [5, 6]. Metal oxides have shown great importance in various applications due to their capability to absorb light [7]. Therefore, loading such metal oxide nanoparticles into natural platforms such as glass substrates. Catalysis, molecular sensing, and environmental remediation are just a few of the many uses for metal and metal oxide nanoparticles [8] . A variety of uses for metal oxides have been investigated[9]. In the early transition metal oxides, a wide range of features were observed, including catalysis, electro-optic and electro-mechanical behavior as well as ferroelectric and wave density charging characteristics [10]. Selective oxidation and dehydration, for example, are made possible by these features. Metal oxide materials are available for use. also garnered a significant amount of focus within the realm of biomedical research because of their unique physicochemical features [11].

The remarkable optical and electrical features of bismuth oxide (Bi_2O_3), an essential broad band-gap of metal oxide semiconductor, good photoconductivity, high dielectric permittivity, and a high refractive index are some of its notable characteristics, have drawn a lot of attention [12]. Researchers have looked into the usage of bismuth oxides in a large number of different uses, fuel cells being one of them, sensors, oxide varistors, and ionic conductors, because of their unusual characteristics [13]. Bi_2O_3 is nontoxic, A simple and inexpensive a type of a type of semiconductor that possesses a band gap of between 2 and 3.9 eV, it is well-known as a p-type semiconductor [14]. There have been several successful strategies reported in recent years with the purpose of creating Bi_2O_3 in a variety of morphologies, including quantum dots nanoparticles, with methods such as microwave-assisted synthesis, electrodeposition, and chemical vapour deposit, it is possible to produce nanobeads, nanorods, nanotubes, nanofibers, and thin films. (CVD) [13].

Since the dawn of time, zinc oxide has already been a utilized in a diverse array of different contexts, and its annual production presently exceeds one and a half million tons [15]. ZnO presents owing to its outstanding optical quality, stability, and piezoelectric qualities, among other things Examples of these include photovoltaic cells, gas sensors, transparent conducting materials, surface acoustic wave devices, and piezoelectric transducers. are some examples of recent advances in the field of electronics are some examples of recent advances in the field of electronics are just a few of the many applications for them [16]. Oxide semiconductors with a high band gap can be used as thin zinc oxide ZnO sensors to detect certain lighting and gases. When it comes to sophisticated applications like window layers Heterojunction solar cells use thin sheets of zinc oxide as one of the most extensively used transparent conducting oxides, as do heat mirrors and piezoelectric devices. For the most part, solar radiation can pass through ZnO because of its high 3.3 eV direct optical energy gap. Furthermore, ZnO's abundance in nature, which lowers its cost, and its high UV-cutoff, which enables it to be used in a diverse range of products and processes [17].

2. Computational details

This aspect focuses on the experimental details used in the fabrication and examination of pure Bi_2O_3 thin films doped with different doping ratios of ZnO (0.0012, 0.0024, 0.0036 and 0.0048) by weight by thermal evaporation method on glass substrates. Optical measurements of thin films such as absorbance (A), (transmittance (T), coefficient of sorption (α), optical. energy gap (Eg), The results were calculated within the range (200-1100 nm) of the spectral range as measured by a spectrophotometer with a dual-beam laser (Shimadzu, UV-1800 A0, Japan), The dielectric characteristics of nanocomposites (Bi_2O_3/ZnO) films were examined by Fourier transformation-infrared spectroscopy (FT-IR) with the range (400–4000) cm^{-1}, and dielectric characteristics at (f = 100 Hz to 5 MHz) by (HIOKI 3532–50 LCR HI TESTER) LCR meter.

Absorbance can [be defined as the ratio between the light intensity that is absorbed by a material (I_A) and the light intensity that is incident on the material (I_o) following the equation [18];

$$A = \frac{I_A}{I_o} \qquad (1)$$

The transmittance, denoted by the symbol T, can be computed by dividing the intensity of the rays that are transmitted from the surface by the intensity of the rays that are incident on it. This ratio can be found by using the formula [19];

$$[T = \exp[-2.303\ A]\ ] \qquad (2)$$

Depending on the direction of incident wave diffusion, an absorption coefficient can be thought of as a reduction in the flux of incident ray energy as a percentage of a distance unit. Photon energy, material characteristics, and the type of electronic transitions are all factors that affect absorption coefficient (α). This equation shows how the absorption coefficient (α) is affected by these factors [20];

$$E = h\upsilon \qquad (3)$$

Transmittance is given by the following equation In cases when the incident photon energy is lower than the energy gap that is banned:

$$T = (1-R)^2 . e^{-\alpha t} \qquad (4)$$

If the intensity of the incident ray (I_o) that hits the blend film material of thickness (t) is given by the Lambert's law, then the intensity of the transmittance ray (I) is determine [21]:

$$I = I_o\ exp(-\alpha t) \qquad (5)$$

The absorption coefficient is expressed by cm^{-1}.

$$\alpha t = 2.303\ log\ I/I_o \qquad (6)$$

where The logarithm of (I/I_0) is the absorbance (A).

The using the following equation to calculate the absorption coefficient [22];

$$\alpha = 2.303(A/t) \qquad (7)$$

In this work a direct transmission occurs between conduction band (C.B) extends precisely above the valence band (V.B) It can be calculated by the equation [23]:

$$\alpha h\upsilon = B\ (\ h\upsilon - E_g{}^{opt})^r \qquad (8)$$

where B is constant, regardless on the kind of material, is the Incident photon frequency, where r is an exponential constant whose value varies depending on the type of transition; r equals 1/2 for the approved direct transition, and r equals 3/2 for the forbidden direct transfer.

The dielectric constant, $\mathcal{E}'$, is given by [24, 25];

$$\mathcal{E}' = \frac{C_p d}{\mathcal{E}_o A} \qquad (9)$$

wherein, C_p is material capacitance, thickness (d in cm), and A=(in cm^2)

The formula for determining dielectric loss $\mathcal{E}''$ is [26, 27];

$$\mathcal{E}'' = \mathcal{E}'\ D \qquad (10)$$

440

wherever, D stands for the distribution factor. The factors that determine the electrical conductivity of A.C are[28][29];

$$\sigma_{a.c} = w\varepsilon''\varepsilon_\circ \tag{11}$$

3. Results and discussions

Figure 1 depicts the X-ray powder diffraction (XRD) patterns for pure Bi2O3 and Bi2O3-doped ZnO thin films. A peak was seen at $2\theta = 27.41°$, which corresponds to the ($\bar{1}21$) for pure Bi_2O_3 from the Joint Committee for Powder Diffraction Standard (JCPDS) card file data (79-2205)[30]. The results are consistent with the studies undertaken by [31]. This shows that both pure and doped Bi_2O_3 films generated by the thermal evaporation mathods had a good c-axis alignment perpendicular to the substrate, a monoclinic wurtzite-type crystal structure, and the behavior of increasing film crystallinity. Using Scherer's method, the crystallite size of the pure Bi2O3 and Bi_2O_3-doped ZnO thin film was determined from the ($\bar{1}21$) diffraction peak using the following equation [32]:

$$D = 0.9\lambda / \beta \cos\theta \tag{12}$$
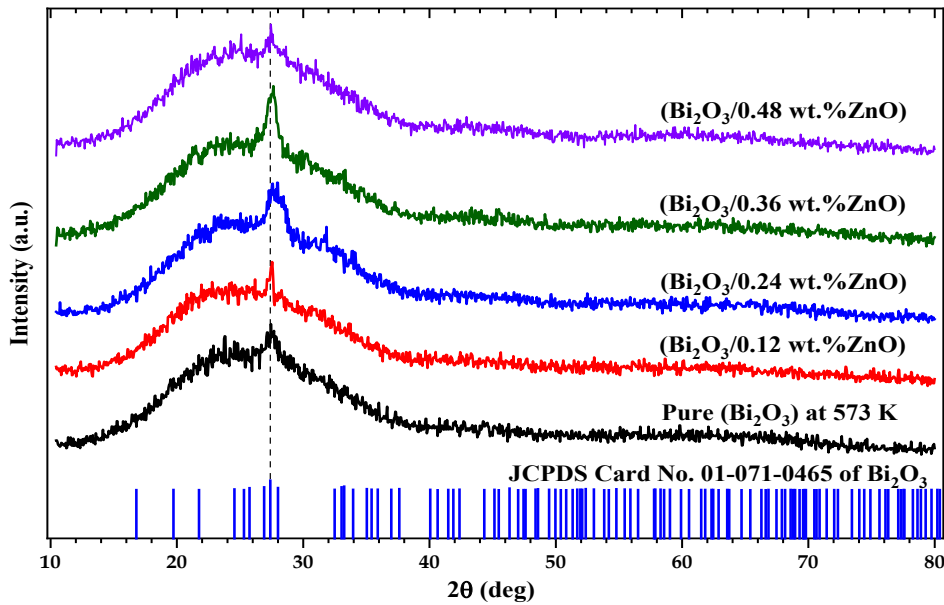
Fig. 1. XRD analysis of (Bi₂O₃/ZnO) thin films at 573K.

The samples' measured FWHM ranged from 0.492° to 0.984°. Our results correspond well with those reported by [33]. The predicted crystallite size range for pure Bi_2O_3 and Bi_2O_3-doped ZnO thin films produced on a glass substrate is 17.348 to 8.674 nm. The results are listed in Table 1.

Table 1. The obtained results of the X-ray powder diffraction (XRD) for pure Bi₂O₃ and Bi₂O₃/ ZnO-doped thin films.

Con. ZnO (wt%)	hkl	$2\theta^0$	d-spacing (A^0)	β^0	β (rad)	D (nm)
Pure	(-121)	27.41323	3.25358	0.492	0.00859	17.34853
0.12%	(-121)	27.54140	3.23605	0.960	0.01676	8.89355
0.24%	(-121)	27.41140	3.25379	0.984	0.01717	8.67423
0.36%	(-121)	27.52922	3.23745	0.840	0.01466	10.16380
0.48%	(-121)	27.40939	3.25403	0.984	0.01717	8.67419

FT-IR analysis was done. To evaluate the distribution of structural bonds in the studied glasses. Figure 2 displays the changes in FT-IR spectra of all glasses . The Bi_2O_3 NPs predominated in the FT-IR spectra of the coupling nanocomposite's spectra. Specifically, the bands in the region from $649.97cm^{-1}$ into $923.84cm^{-1}$ correspond to the overlapping stretching vibrations of Bi–O bonds of BiO_6 coordination octahedra and Zn–O bonds. In addition, weak to medium bands at $1126.35cm^{-1}$ and $1421.44cm^{-1}$ and $1575.73cm^{-1}$ can be noticed as the Bi_2O_3 loading in nanocomposites increases. These absorption bands were linked to various types of Bi–O vibrations induced by the interaction of Bi–O bonds with their environment. Similarly to the ZnO bands, the characteristic bands at $3421.48cm^{-1}$ got stronger with increased Bi_2O_3 loading in the nanocomposite, indicating a higher –OH group density on the catalyst's surface. The absorption peaks seen around $3421.48cm^{-1}$ are attributed to O–H stretching vibrations, which are typical in oxide glass due to water trapping of raw materials from the surrounding atmosphere [34, 35].
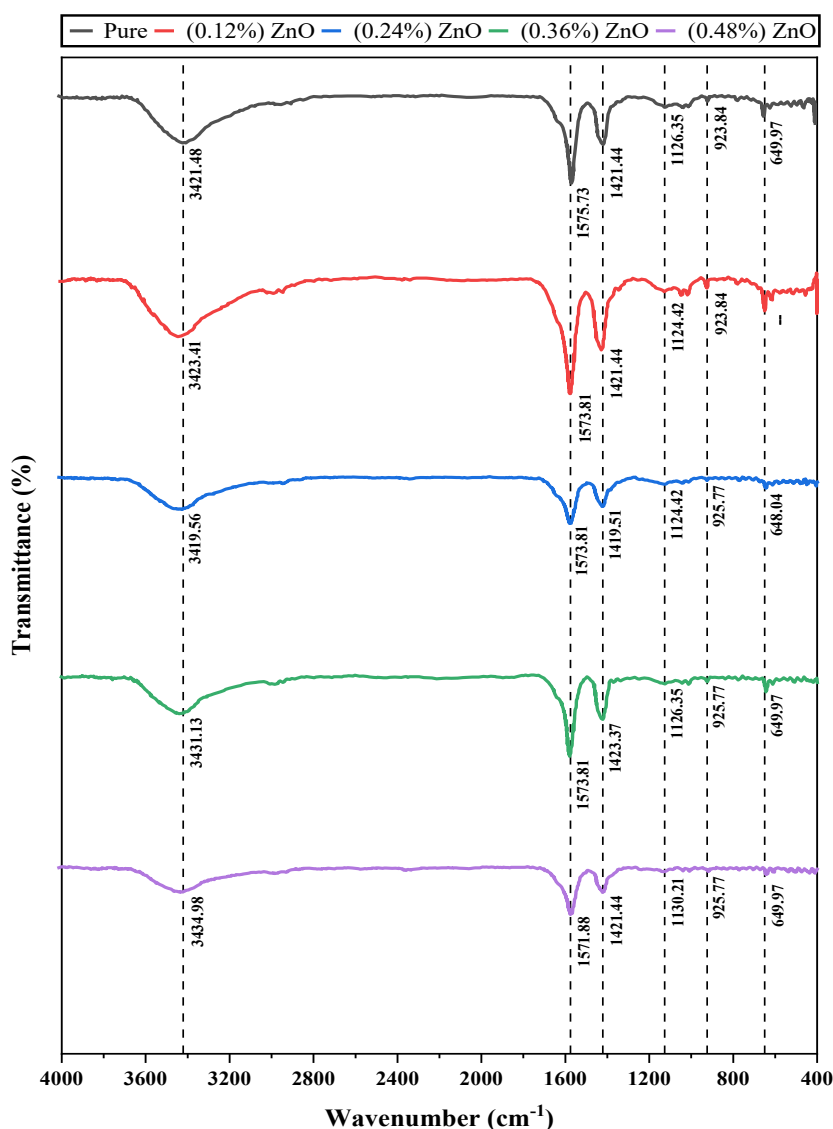
Fig. 2. FT-IR analysis of (Bi₂O₃/ZnO) thin films at 573K.

Figures 3 displaying photos obtained from Nanoparticles in thin films were analyzed using field emission scanning electron microscope (FE-SEM). These findings can be explained by the fact that clusters of nanoparticles form when the concentration of the substance is lower. When there is a higher concentration of ZnO nanoparticles, the Bi_2O_3 is able to support the formation of a

442

network due to the nanoparticles. Matrix This results in an increase in the number of companies offering free shipping [36, 37].
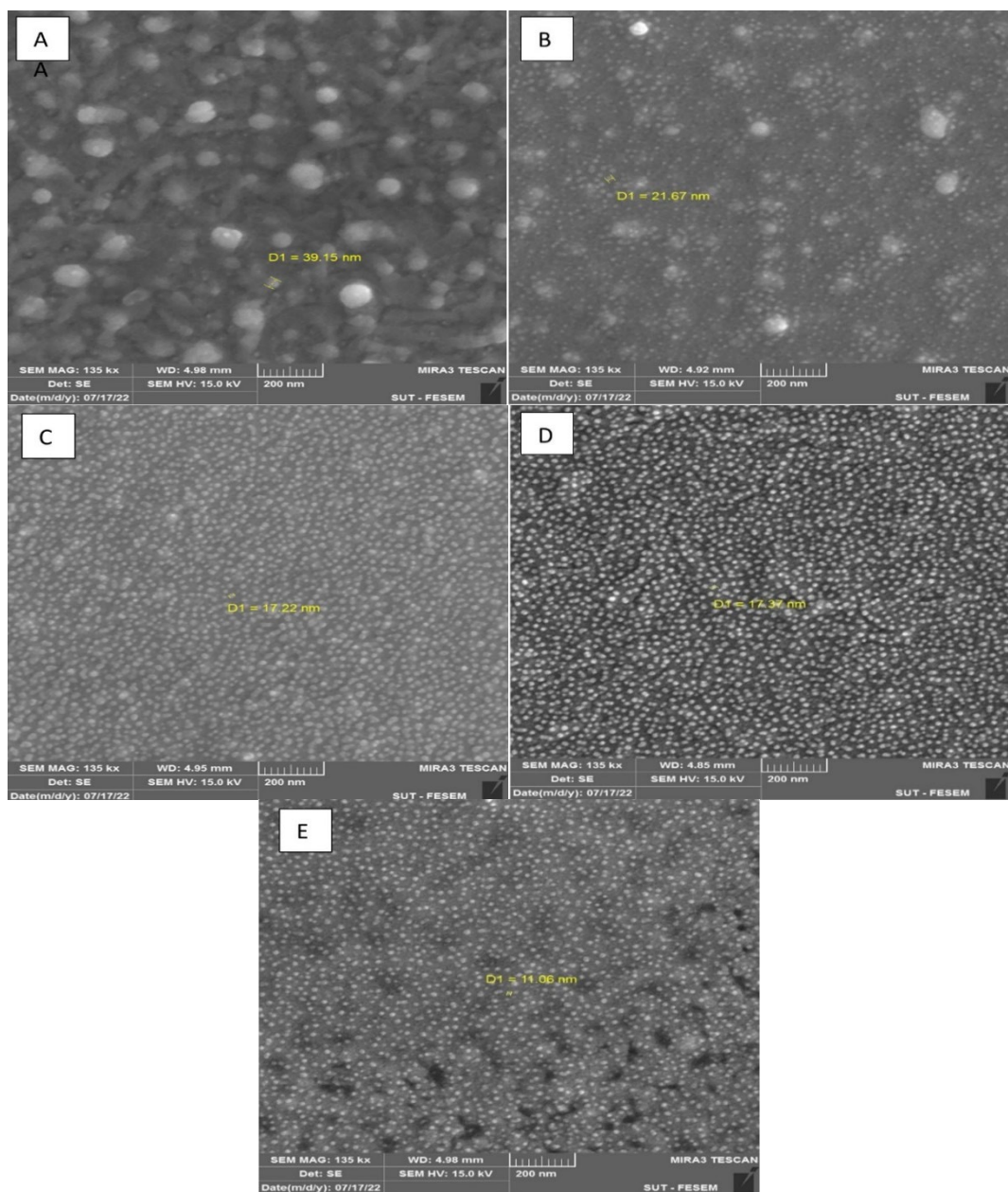
Fig. 3. FE-SEM images of (Bi$_2$O$_3$/ZnO) nanocomposites: A for pure B for 0.12 wt.% (ZnO) NPs, C for 0.24 wt.% (ZnO) NPs, D for 0.36 wt.% (ZnO) NPs and E for 0.48 wt.% (ZnO) NPs.

Absorption (Bi$_2$O$_3$/ZnO) with varied concentration (ZnO) for a wavelength ranging at normal temperature, a wavelength range of (200-1100 nm) was observed. Figure 4 shows the contrast of the optical absorption with the wavelength of (Bi$_2$O$_3$/ZnO). From these numbers it can be seen that the spectra show that the UV absorption in all of these films is larger. The low absorption in the visible range is evident in all nanocomposites. In order to clarify this, we can look at it this way: High-frequency photons do not interact with atoms; hence the photon is transmitted rather than blocked. When the wavelength of light drops (within close proximity to the basic absorption edge), the photon will exhibit the following behavior be absorbed because of the interaction between the incident photon and the substance. Weight (ZnO) percentages improve the

absorption. This is due to the unbound electrons absorbing the incident light. The findings here are consistent with those of other researchers [38, 39].
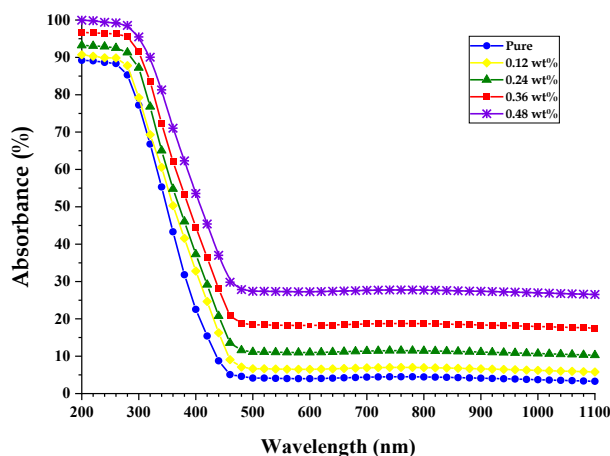
Fig. 4. The absorbance as function of wavelength for (Bi$_2$O$_3$/ZnO) thin films.

Figure 5 is a graph that displays the transmittance (T) as a function of the wavelength. of (Bi$_2$O$_3$/ZnO). Optical transmittance spectra of thin films different concentration of ZnO nanoparticles. It is evident that the transmittance increases as the wavelength of various concentrations increases and decreases as the concentration of ZnO nano-doping increases [40]. The findings here are consistent with those of other researchers [41] .
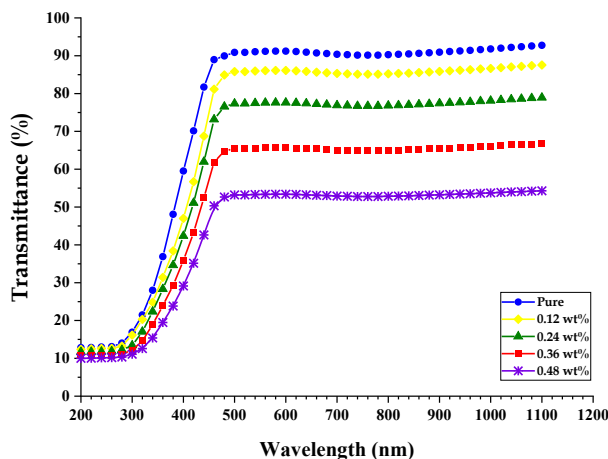
Fig. 5. The transmittance as function of wavelength for (Bi$_2$O$_3$/ZnO) thin films.

Figure 6 Absorption coefficient is plotted against wavelength for thin films (Bi$_2$O$_3$/ZnO). At longer wavelengths, the absorption coefficient is at its lowest value and low energies, as can be observed. Electron transition is not possible because the photon's energy is insufficient to move electrons moving electrons from the valence band to the conduction band in a semiconductor material [42].

Absorption is excellent at high energies, which indicates a high chance of electron transitions. As a consequence of this, the energy of the incident photon is sufficient to force one electron to migrate from the valence band to the conduction band. The energy of the photon that was detected during the incident was greater than the allowed energy gap [43].

A direct electron transition happens when This coefficient is greater than that of absorption, therefore ($\alpha > 10^4$) cm^{-1} at high energies, the energy and moment of the electron and photons are maintained while they travel through the transition. Whereas, at low energies, the absorption coefficient values ($\alpha < 10^4$) cm^{-1} are likely to occur, resulting in an indirect transition of electrons, and the phonon helps sustain the electronic momentum [44].

Among other results, the thin-film absorption coefficient (Bi_2O_3/ZnO) is greater than (10^4) cm^{-1}. This shows that electron transfers are direct. This result is similar to the results of the other researcher [41].
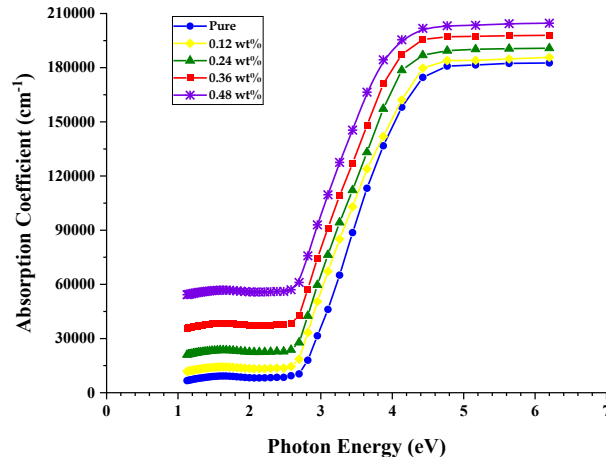
Fig. 6. The absorption coefficient as a function of photon energy for (Bi_2O_3/ZnO) thin films.

Equation (8) has been used to compute both the permitted and prohibited direct transition band energy gap. The energy gap of the direct transition band is calculated when r =1/2, when this is done, the energy gap in the forbidden indirect transition band can be determined r=3/2.

Absorption edge (hv)^2 for (Bi_2O_3/ZnO) is shown in Figure 7 depending on the amount of photon energy present when the (hv)^2 = 0 value is drawn from the upper half of the curve toward the (x)-axis, The energy gap of both pure Bi_2O_3 and Bi_2O_3-doped ZnO with different ratios (0.0012, 0.0024, 0.0036 and 0.0048) wt% with a thickness of 50 nm is shown on. An evident decrease in the Energy gap values is observed with the increase of the ZnO ratio. This preposition increase explains that Bi_2O_3/ZnO valence band electrons are transferred to conduction band electrons through the Borstein-Moss effect, which is a type of semiconductor film where the Fermi level is positioned in the conductive band and an electron shield flows to these levels, resulting in the transfer of electrons. According to Table (2), the Eg values are listed. The findings of the second researcher are very comparable to this one [45].

Table (2) explain how the direct energy gap's prohibited transition is determined, in the same manner Fig 8 depicts the forbidden transition of the direct energy gap between and (Bi_2O_3/ZnO). These findings are in accordance with what the researcher had expected to see [45].
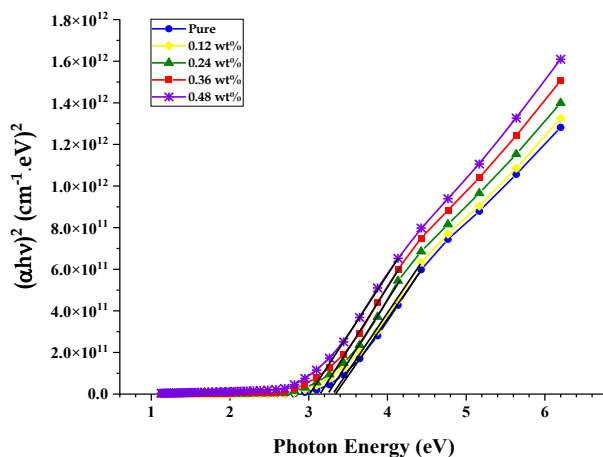
Fig. 7. Optical energy gap for the allowed direct transition $(\alpha h\upsilon)^2$ versus photon energy of (Bi_2O_3/ZnO).
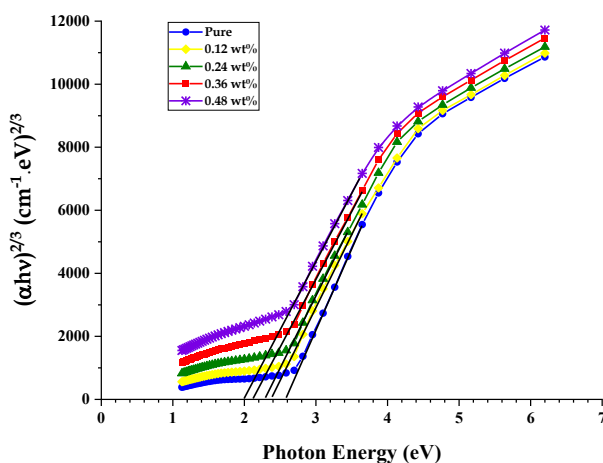
Fig. 8. Optical energy eap for the forbidden direct transition $(\alpha h\upsilon)^{3/2}$ versus photon energy of (Bi_2O_3/ZnO).

Table 2. For (Bi_2O_3/ZnO) thin films, the values of the energy gap for the permissible and banned direct transitions.

Zinc Oxide	$E_g(eV)$	
	Allowed	**Forbidden**
0	3.18	3.01
0.0012	2.86	2.78
0.0024	2.82	2.61
0.0036	2.81	2.45
0.0048	2.63	2.42

Figure 9 Due to the ability of dipoles in nanocomposites specimens to rotate in the direction of the applied electric field and the reduction of space charges or interfacial polarization to overall polarization, decreases with increasing frequency for all samples [46, 47]. Variation of 'ε for thin films (Bi_2O_3/ZnO) NPs content at 100Hz is shown in Figure 10. Observations indicate that increases with increasing ZnO content for all samples. which is Inter polarization within the thin films in the alternating applied field Electric field and height of charge carriers can characterize the actions.

Which means that prepared nanocomposites have low loss, meaning low energy loss which make it suitable for nanoelectronics devices applications.
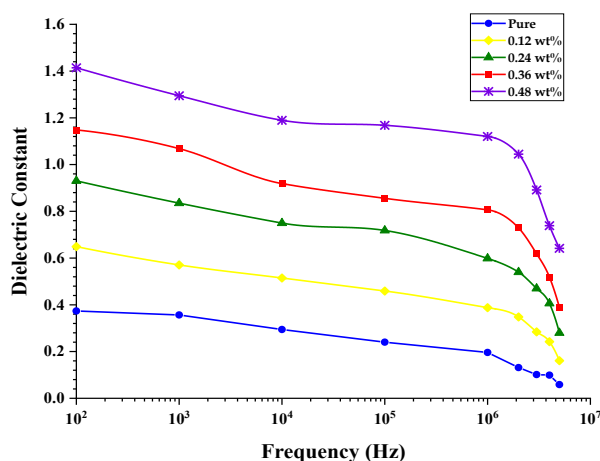
Fig. 9. Variation of Ɛ' with frequency of (Bi₂O₃/ZnO) thin films.
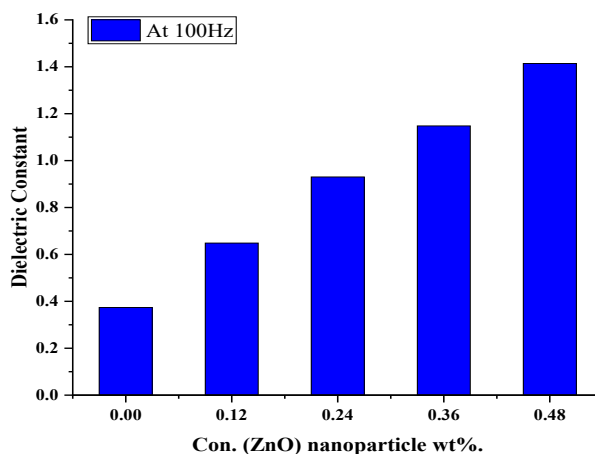
Fig. 10. Effect of ZnO NPs content on dielectric constant of Bi₂O₃.

Figure 11 shows the ε'' behavior of (Bi$_2$O$_3$/ZnO) thin films with frequency. It was observed that reduce ε'' With a higher frequency, which is due to the reduction of the polarization of the influence of space charges. When the frequency is low, ε'' has a high value, but as the frequency goes up, it goes down. This is because the dipoles have time to line up the electric field before it changes direction [48].

Figure 12 displays the influence that the presence of ZnO NPs has on the dielectric loss of Bi$_2$O$_3$ when measured at 100 Hz. Because of the high nanoparticle concentration, there is an increase in values, which can be linked to the rise of the number of charge carriers in the system having a relatively modest concentration of nanoparticles yet a significant amount of clusters generated. These results are in agreement with [49].
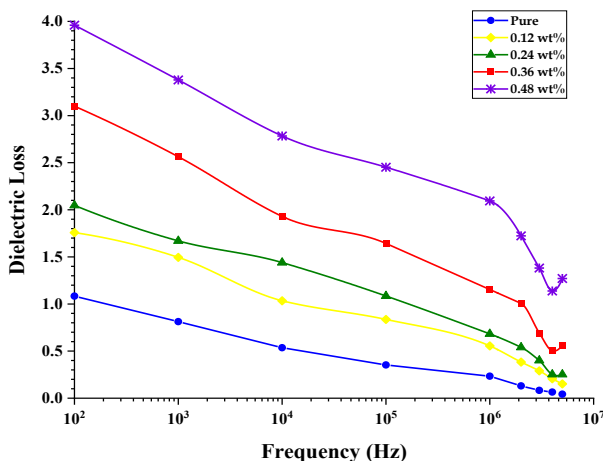
Fig. 11. Variation of ε'' with frequency of (Bi₂O₃/ZnO) thin films.
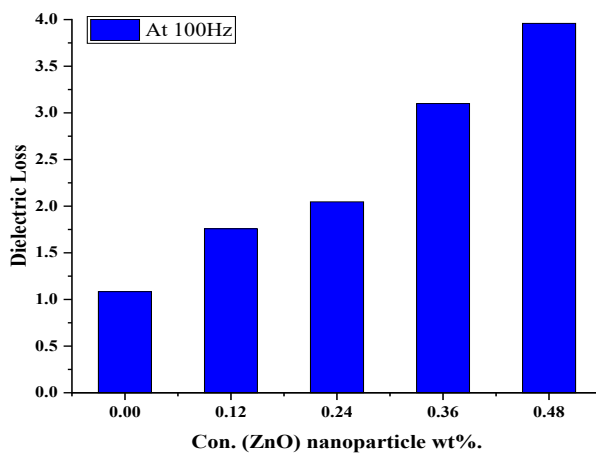
Fig. 12. Effect of ZnO NPs content on dielectric loss of Bi₂O₃.

Fig. 13 As shown this Figure, the mobility of charge carriers and the hopping of ions from the cluster are linked to the fact that the A.C. of (Bi₂O₃: ZnO) thin films increases as the frequency does [50].

Figure 14 exhibits the A.C conductivity of (Bi₂O₃/ZnO) thin film with content of NPs at 100 Hz. From figure (14), it is noted that the $\sigma_{A.C}$ raisings with raising of (ZnO) NPs concentration which due to raise in the number of charge carriers[45].
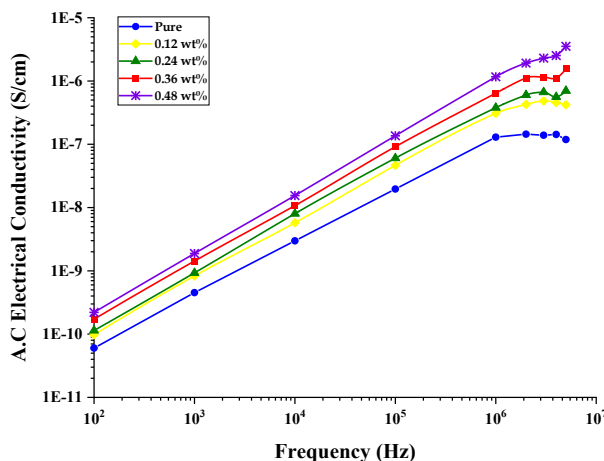
Fig. 13. Variation of A.C conductivity with frequency of (Bi₂O₃/ZnO) thin films.
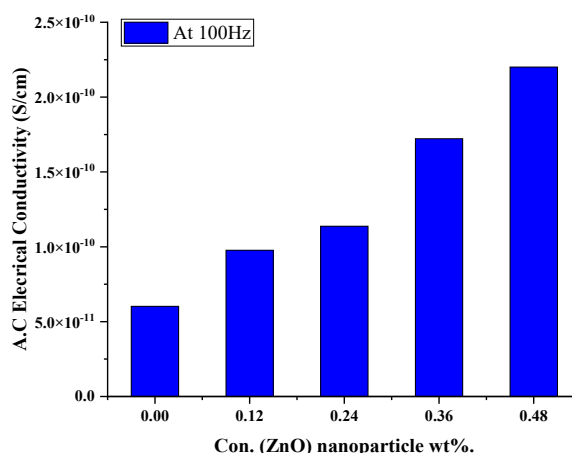
Fig. 14. Effect of ZnO NPs ratio on A.C conductivity of Bi_2O_3 at 100 Hz.

The culmination of the investigations into the dielectric characteristics, which It is possible to consider the dielectric constant, the dielectric loss, and the electrical conductivity of the suggested (Bi_2O_3/ZnO) nanostructures as the fabricated thin films. Promising materials in different domains of nanoelectronics and sensors.

4. Conclusions

This work includes studying the structural and dielectric characteristics of (Bi_2O_3/ZnO) thin films for use in various nanoelectronics and sensor applications. From XRD, the crystalline was satisfied with a monoclinic wurtzite structure and preferential orientation in the ($\bar{1}21$) direction. The crystallite size increased with the increasing of ZnO doping. The FT-IR confirmed no interaction between (Bi_2O_3/ZnO) NPs and FE-SEM, confirming that (ZnO) NPs Uniform distribution within Bi2O3.The absorbance of the thin films (Bi_2O_3/ZnO) increases with the increase of the nanoparticles (ZnO) concentrations. While the Transmittance and energy gap of the direct transfer (allowed, forbidden) of the (Bi_2O_3/ZnO) thin films decreases with the increase of the concentrations of (ZnO) nanoparticles.

The insulating characteristics of the (Bi_2O_3/ZnO) A.C thin films indicated mixed with the increase in the content of (ZnO) NPs. The dielectric constant and dielectric loss go down while A.C electrical conductivity alternating current increases when Frequency increases of Bi_2O_3.

Acknowledgments

References

[1] L. A. Kolahalam, I. V. Kasi Viswanath, B. S. Diwakar, B. Govindh, V. Reddy, Y. L. N. Murthy, Mater. Today Proc., vol. 18, no. xxxx, pp. 2182-2190, 2019; https://doi.org/10.1016/j.matpr.2019.07.371

[2] H. S. Nalwa, Handbook of nanostructured materials and nanotechnology, five-volume set. Academic Press, 1999.

[3] S. Logothetidis, Nanostructured materials and their applications. Springer Science & Business Media, 2012; https://doi.org/10.1007/978-3-642-22227-6

[4] K. M. M. Abou El-Nour, A. Eftaiha, A. Al-Warthan, and R. A. A. Ammar, Arab. J. Chem., vol. 3, no. 3, pp. 135-140, 2010; https://doi.org/10.1016/j.arabjc.2010.04.008

[5] R. Kumar, W. Zheng, X. Liu, J. Zhang, and M. Kumar, Adv. Mater. Technol., vol. 5, no. 5, pp. 1-28, 2020; https://doi.org/10.1002/admt.201901062

[6] X. Liu, T. Ma, N. Pinna, and J. Zhang, Adv. Funct. Mater., vol. 27, no. 37, pp. 1-30, 2017; https://doi.org/10.1002/adfm.201702168

[7] N. A. Ibrahim, Nanomaterials for Antibacterial Textiles. Elsevier Inc., 2015; https://doi.org/10.1016/B978-0-12-801317-5.00012-8

[8] Z. Yang, H. Peng, W. Wang, and T. Liu, J. Appl. Polym. Sci., vol. 116, no. 5, pp. 2658-2667, 2010; https://doi.org/10.1002/app.31787

[9] S. Murthy, P. Effiong, and C. C. Fei, Metal oxide nanoparticles in biomedical applications. INC, 2020; https://doi.org/10.1016/B978-0-12-817505-7.00011-7

[10] G. A. Kontos et al., Express Polym Lett, vol. 1, no. 12, pp. 781-789, 2007; https://doi.org/10.3144/expresspolymlett.2007.108

[11] S. Laurent, S. Boutry, and R. N. Muller, Metal Oxide Particles and Their Prospects for Applications. Elsevier Ltd., 2018; https://doi.org/10.1016/B978-0-08-101925-2.00001-2

[12] L. Leontie, M. Caraman, M. Delibaş, and G. I. Rusu, Mater. Res. Bull., vol. 36, no. 9, pp. 1629-1637, 2001; https://doi.org/10.1016/S0025-5408(01)00641-9

[13] L. Zhang, Y. Hashimoto, T. Taishi, I. Nakamura, and Q. Q. Ni, Appl. Surf. Sci., vol. 257, no. 15, pp. 6577-6582, 2011; https://doi.org/10.1016/j.apsusc.2011.02.081

[14] H. Oudghiri-Hassani et al., J. Taibah Univ. Sci., vol. 9, no. 4, pp. 508-512, 2015; https://doi.org/10.1016/j.jtusci.2015.01.009

[15] A. Moezzi, A. M. McDonagh, and M. B. Cortie, Chem. Eng. J., vol. 185-186, pp. 1-22, 2012; https://doi.org/10.1016/j.cej.2012.01.076

[16] W. Gao and Z. Li, Ceram. Int., vol. 30, no. 7, pp. 1155-1159, 2004; https://doi.org/10.1016/j.ceramint.2003.12.197

[17] M. K. Khalaf, B. T. Chiad, A. F. Ahmed, and F. A. H. Mutlak, Int. J. Appl. Innov. Eng. Manag, vol. 2, no. August 2019, pp. 178-184, 2013.

[18] N. A. Hassan and I. H. Khudayer, AIP Conf. Proc., vol. 2190, no. December, 2019; https://doi.org/10.1063/1.5138536

[19] PanelA.M.TalebA.J.H.Al-Wattar, Sol. Wind Technol. Vol. 5, Issue 5, 1988, Pages 503-515, vol. 5, no. 5, 1988; https://doi.org/10.1016/0741-983X(88)90041-0

[20] R. Enderlein and N. J. M. Horing, Fundamentals of semiconductor physics and devices. World Scientific, 1997; https://doi.org/10.1142/2866

[21] D. R. Tobergte and S. Curtis, The Physics of Thin Film Optical Spectra: An Introduction, vol. 53, no. 9. 2013.

[22] O. S. Heavens, Optical properties of thin solid films. Courier Corporation, 1991.

[23] C. Kittel, P. McEuen, and P. McEuen, Introduction to solid state physics, vol. 8. Wiley New York, 1996.

[24] A. S. Haiba, O. E. Gouda, S. F. Mahmoud, and A. A. El-gendy, TELKOMNIKA (Telecommunication Comput. Electron. Control., vol. 12, no. 4, pp. 763-772, 2014; https://doi.org/10.12928/telkomnika.v12i4.115

[25] M. H. Meteab, A. Hashim, and B. H. Rabee, Silicon, no. 0123456789, 2022; https://doi.org/10.1007/s12633-022-02020-y

[26] M. O. Farea, A. M. Abdelghany, and A. H. Oraby, RSC Adv., vol. 10, no. 62, pp. 37621-37630, 2020; https://doi.org/10.1039/D0RA07601E

[27] H. Shivashankar, K. A. Mathias, P. R. Sondar, M. H. Shrishail, and S. M. Kulkarni, J. Mater. Sci. Mater. Electron., vol. 32, no. 24, pp. 28674-28686, 2021; https://doi.org/10.1007/s10854-021-07242-1

[28] M. H. Meteab, A. Hashim, and B. H. Rabee, Silicon, pp. 1-12, 2022; https://doi.org/10.1007/s12633-022-02114-7

[29] H. S. Suhail and B. H. Rabee, AIP Conf. Proc., vol. 2213, no. March, 2020; https://doi.org/10.1063/5.0000093

[30] P. D. File, Joint committee on powder diffraction standards, ASTM, Philadelphia, Pa, pp. 9-185, 1967.

[31] A. K. Sahoo and M. R. Panigrahi, Bull. Mater. Sci., vol. 44, no. 3, pp. 1-9, 2021; https://doi.org/10.1007/s12034-021-02515-1

[32] K. H. Abass and M. K. Mohammed, Nano Biomed. Eng., vol. 11, no. 2, pp. 170-177, 2019; https://doi.org/10.5101/nbe.v11i2.p170-177

[33] B. C. Dev, M. H. Babu, J. Podder, S. Sagadevan, and A. Zubair, " J. Mater. Sci. Mater. Electron., vol. 30, no. 16, pp. 15670-15682, 2019; https://doi.org/10.1007/s10854-019-01950-5

[34] M. K. Halimah, A. Azuraida, M. Ishak, and L. Hasnimulyati, J. Non. Cryst. Solids, vol. 512, no. March, pp. 140-147, 2019; https://doi.org/10.1016/j.jnoncrysol.2019.03.004

[35] S. M. Lam, J. C. Sin, A. Z. Abdullah, and A. R. MohamedWater. Air. Soil Pollut., vol. 224, no. 5, 2013; https://doi.org/10.1007/s11270-013-1565-6

[36] A. C. Mohan and B. Renjanadevi, Procedia Technol., vol. 24, pp. 761-766, 2016; https://doi.org/10.1016/j.protcy.2016.05.078

[37] R. I. Kamel, D. S. Ahmed, and U. M. Nayef, Optik (Stuttg)., vol. 193, no. June, p. 163013, 2019; https://doi.org/10.1016/j.ijleo.2019.163013

[38] A.Oreibi, A.Oreibi M.Sc. thesis ,College of Education for pure sciences, University of Babylon ,(2018) ., p. 2018, 2018.

[39] S. Sharma, R. Vyas, and Y. K. Vijay, Advanced Materials Research, 2012, vol. 585, pp. 139-143; https://doi.org/10.4028/www.scientific.net/AMR.585.139

[40] B. Rabee, M. Habeeb, and A. Hashim, Int. J. Sci. Res., vol. 3, pp. 2319-7064, 2014.

[41] I. Dhahri et al., Ceram. Int., vol. 48, no. 1, pp. 266-277, 2022; https://doi.org/10.1016/j.ceramint.2021.09.101

[42] A. D. Ghaleb Abdul Wahab, N. N. Hussein, B. Ahmed, and T. Rafia, Br. J. Sci, vol. 4, pp. 117-124, 2012.

[43] D. K. Eric, Engines of Creation. The Coming Era of Nanotechnology, Anchor B., 1986.

[44] M. Crane, Sol. Cells, Collage Educ. Univ. Mousl, 1989.

[45] Y. Al-Hadeethi, M. I. Sayyed, and Y. S. Rammah, Ceram. Int., vol. 45, no. 16, pp. 20724-20732, 2019; https://doi.org/10.1016/j.ceramint.2019.07.056

[46] H. J. Youn, T. Sogabe, C. A. Randall, T. R. Shrout, and M. T. Lanagan, J. Am. Ceram. Soc., vol. 84, no. 11, pp. 2557-2562, 2001; https://doi.org/10.1111/j.1151-2916.2001.tb01053.x

[47] L. X. Li, Y. X. Jin, H. L. Dong, S. H. Yu, and D. Xu, Ceram. Int., vol. 40, no. PB, pp. 16133-16139, 2014; https://doi.org/10.1016/j.ceramint.2014.07.044

[48] J. Massera et al., J. Non. Cryst. Solids, vol. 356, no. 52-54, pp. 2947-2955, 2010; https://doi.org/10.1016/j.jnoncrysol.2010.03.045

[49] H. Du, X. Yao, and L. Zhang, Ceram. Int., vol. 28, no. 3, pp. 231-234, 2002; https://doi.org/10.1016/S0272-8842(01)00084-0

[50] J. S. Ashwajeet and T. Sankarappa, Ionics (Kiel)., vol. 23, no. 3, pp. 627-636, 2017; https://doi.org/10.1007/s11581-016-1819-6